Cytoskeleton

Inhibition of myosin II triggers morphological transition and increased nuclear motility in cell culture

Journal:	*Cytoskeleton*
Manuscript ID:	CSK-10-058.R1
Wiley - Manuscript type:	Research Article
Date Submitted by the Author:	n/a
Complete List of Authors:	Szabo, Balint; Eotvos University, Biological Physics Unnep, Renata; Eotvos University, Biological Physics Marko, Karoly; Hungarian Academy of Sciences, Experimental Medicine Kornyei, Zsuzsanna; Hungarian Academy of Sciences, Experimental Medicine Mehes, Elod; Eotvos University, Biological Physics Czirok, Andras; University of KS Med Ctr, Anatomy & Cell Biology; Eotvos University, Biological Physics
Keywords:	interkinetic nuclear migration, radial glia, centrosome, tensegrity, traction force

Inhibition of myosin II triggers morphological transition and increased nuclear motility

Bálint Szabó[1], Renáta Ünnep[1], Károly Markó[2], Zsuzsanna Környei[2], Előd Méhes[1] and András Czirók[1,3]

1 Department of Biological Physics, Eotvos University, Budapest, Hungary

2 Institute of Experimental Medicine, Hungarian Academy of Sciences, Budapest, Hungary

3 Department of Anatomy & Cell Biology, University of Kansas Medical Center, Kansas City, KS, USA

February 11, 2011

Key words: interkinetic nuclear migration, radial glia, centrosome, tensegrity, blebbistatin, traction force

Abstract

We investigate the effect of myosin II inhibition on cell shape and nuclear motility in cultures of mouse radial glia-like neural progenitor and rat glioma C6 cells. Instead of reducing nucleokinesis, the myosin II inhibitor blebbistatin provokes an elongated bipolar morphology and increased nuclear motility in both cell types. When myosin II is active, time-resolved traction force measurements indicate a pulling force between the leading edge and the nucleus of C6 cells. In the absence of myosin II activity, traction forces during nucleokinesis are diminished below the sensitivity threshold of our assay. By visualizing the centrosome position in C6 cells with GFP-centrin, we show that in the presence or absence of myosin II activity the nucleus tends to overtake or lag behind the centrosome, respectively. We interpret these findings with the help of a simple viscoelastic model of the cytoskeleton consisting active contractile and passive compressed elements.

Introduction

Nucleokinesis, the movement and positioning of the cell nucleus, is an essential process within a diverse variety of organisms and cell types (Morris, 2000). Specialized nuclear movements occur in yeasts during cell division (Tran et al., 2001; Ding et al., 1998), as well as during complex organ development like in the case of Drosophila ommatidia (Mosley-Bishop et al., 1999; Whited et al., 2004). Nucleokinesis has been extensively documented in the developing vertebrate brain. Migration of neurons and neural progenitors can be readily divided into two independent phases: extension of the leading process and repositioning of the nucleus with or without substantial overall displacement of the elongated cell body (Tsai and Gleeson, 2005). Interkinetic nuclear migration (INM) is another spectacular example of nucleokinesis: in the ventricular zone of the developing vertebrate brain asymmetric cell divisions are coupled to an intriguing oscillating nuclear movement of neuroepithelial and radial glial cells (Frade, 2002; Murciano et al., 2002; Schenk et al., 2009). Genetic defects effecting nucleokinesis can result in severe developmental diseases like lissencephaly (Tsai et al., 2005, 2007; Shu et al., 2004).

While the microtubular network is clearly implicated in nucleokinesis within all animal cells or fungi investigated, the various cell types appear to utilize distinct molecular machineries (Morris, 2003). In yeasts (Tran et al., 2001), Dictyostelium (Brito et al., 2005) and artificial models (Holly et al., 1997) the astral microtubule system can act as a positioning device. Microtubule associated motors, usually cortical dyneins located at the distal ends of astral microtubules are implicated in nuclear positioning during cell division in early C. elegans (G¨onczy et al., 2000) and Drosophila embryos (Robinson et al., 1999). In such systems, the asymmetric (polarized) activity of cortically-localized motors may generate the force which moves and positions the nucleus (Ahringer, 2003). In neurons both cytoplasmic dynein and myosin II motors are thought to play a role in nucleokinesis (Schaar and McConnell, 2005; Tsai et al., 2007).

Despite the developmental and functional importance of nuclear positioning in vertebrate cells, the underlying mechanics of force generation is not well explored (Kole et al., 2005; Rowat et al., 2008). In addition to microtubule-based positioning mechanisms, similar to that of yeasts and dictyostelium, one may also consider nuclear movement in the context of cell locomotion. During cell migration the cell body is translocated by a concerted action of actin-myosin contractile filaments (Munevar et al., 2001; Pan et al., 2009). Therefore, myosin II is a natural candidate for force generation during nucleokinesis of tissue cells. The complex nature of nuclear movement, however, is indicated by the different, sometimes contradictory mechasims proposed recently. In vitro studies of cerebellar granule neurons suggested that acto-myosin contractility pulls the nucleus at the proximal area of the leading cell process (Solecki et al., 2009). Another study concluded that the machinery responsible for the apical-to-basal and basal-to-apical phases of INM are different: in the apical-to-basal phase myosin II motors contract the soma and push the nucleus from the rear of the cell, while cytoplasmic dyneins carry the nucleus as a cargo in the opposite direction (Schenk et al., 2009). Nuclei participating in INM were also reported to move along uniformly oriented microtubules, uncoupled from the centrosome (Tsai et al., 2010). This study proposed a mechanism using the Kif1a kinesin motor – instead of myosin II – to drive nuclear movements towards the basal surface of the ventricular zone.

The centrosome, the organizing center of astral microtubules, is also expected to play a role in nucleokinesis. The coupling between the nucleus and centrosome during INM and nucleokinesis is known to be mediated by several proteins (Zhang et al., 2009). If nucleokinetic forces are exerted by astral microtubules, then these forces are transmitted through the centrosome to the nucleus and therefore the position of the centrosome would determine if the nucleus is being pushed or pulled. Even if the role of microtubule organization is not a mechanical one, but instead it sets or maintains front/rear polarity within the cell (Wittmann and Waterman-Storer, 2001; Solecki et al., 2004; Cowan and Hyman, 2004; de Anda et al., 2005), a functional centrosome is still required to provide normal microtubular architecture. As the centrosome position varies with cell types during directed migration (Yvon et al., 2002; Niu et al., 1997; Danowski et al., 2001), the relative position of the centrosome and the nucleus may be less crucial than initially suggested (Umeshima et al., 2007).

In this study we investigate the mechanical aspects of nucleokinesis using mouse radial glia-like and C6 rat glioma cell types in culture. The radial glia-like cell population has been in the focus of research interest as they may function as primary progenitors or neural stem cells (Kriegstein and Alvarez-Buylla, 2009; Pollard and Conti, 2007). Surprisingly, instead of inhibiting nucleokinesis, inhibition of myosin II triggers an increased nuclear motility after a pronounced morphological transition in both cell types. When myosin II is blocked, cells acquire a highly elongated bipolar shape, similar to the cell morphologies obtained on narrow adhesion stripes or to the morphology of the C6-R radial glia-like subclone (Friedlander et al., 1998) of the C6 cell line. The nuclear positioning mechanism was studied using time-lapse recordings of GFP-centrin transfected C6 cells and traction force microscopy.

Materials and Methods

Preparation and maintenance of radial glia-like neural stem cells

Primary neuronal cultures were established from the telencephali of 14-16 day-old CD1 mouse embryos. Cell suspensions were centrifuged (120 g; 10 min) and quickly re-suspended in DMEM/F12 (1/1) medium (Sigma) containing 1% B27 supplement (Gibco). $6x10^6$ cells were plated onto a 60 mm Petri-dish (Falcon) coated with AK-cyclo[RGDfC] (Marko et al., 2008). The culture medium was supplemented with 20 ng/ml EGF (Peprotech). The medium was changed every second day after rapid rinsing with PBS in order to wash off weakly adhering cells. The cultures were harvested by trypsinization on day 6-8. After the first passage, the cultures could be subcultivated on every second or third day. After 3-4 passages, cultures in EGF-containing medium were virtually homogeneous populations of radial glia-like cells. The cultures display radial glia-specific features including nestin-, RC2-immunoreactivity and Pax6, Sox2, Blbp, Glast gene expression. Radial glia-like cells can give rise to neurons, astrocytes and oligodendrocytes (Marko, submitted).

Maintenance and transfection of C6 cells

C6 glioma cells were grown in MEM supplemented with 5% fetal calf serum (FCS), 4 mM glutamine and 40 µg/ml gentamycin (Sigma) in humidified air atmosphere containing 5% CO_2, at 37°C. Cultures reaching semiconfluency were transfected with 4 µg plasmid DNA with SuperFect Transfection Reagent, according to the manufacturer's protocol (Quiagen). The plasmid pJLS148 (GFP-centrin) was a kind gift of J.L. Salisbury (D'Assoro et al., 2001). The transfected cultures were grown in medium containing 800 µg/ml G418. Cultures subjected to continuous selection were used for nuclear motility studies. Cells were plated at a density of 10^4 cells/cm^2.

Inhibitors

For inhibiting myosin II activity, blebbistatin (Sigma) was used at 1, 3, 6, 20 and 50 µM final concentrations. Monastrol (Sigma), an eg5 kinesin inhibitor, was used at 50 µM final concentration. LY294002 (Sigma), a highly selective inhibitor of PI3 kinase, was used at a 20 µM final concentration. These three inhibitors were dissolved in DMSO and added to the medium to reach their respective final concentrations in such a dilution that DMSO did not exceed 0.1%. Control cultures were exposed to 0.1% DMSO or the inactive (+) enantiomer of blebbistatin at 20 µM concentration. Selective Rho kinase (ROCK) inhibitor Y27632 (Sigma) was used in 20 and 40 µM final concentrations. For inhibiting G-actin polymerization into F-actin, latrunculin A (Sigma) was used at 50, 10 and 500 nM final concentrations, whereas for stabilizing F-actin jasplakinolide (Merck) was used in 10, 50 and 100 nM. Microtubule assembly inducer taxol (Merck) was used for stabilizing microtubules at concentrations ranging from 15 to 30 nM and vinblastine (Sigma) was used in 10 to 20 nM final concentrations to inhibit microtubule assembly.

Time-lapse microscopy

Time-lapse recordings were performed on a computer-controlled Leica DM IRB inverted microscope equipped with 10x, 20x and 40x objectives and an Olympus DP70 camera. Cell cultures were kept at 37°C in humidified 5% CO_2 atmosphere within an incubator (www.cellmovie.eu) attached to the microscope stage. Images were acquired every 10 minutes for 2-3 days both in phase contrast and epifluorescence optical modes (Czirok et al., 2002).

Nucleus and centrosome tracking

Cells were identified and tracked through image sequences by an automatic, two-step procedure for nuclear velocity measurements presented in Figs. 3 and 8 and supplementary Fig. S3. In phase contrast images cell nuclei are darker or brighter than the surrounding cell body. Thus, the algorithm loop consisted of a PIV displacement prediction (Zamir et al., 2005) followed by a gradient search for local brightness minima and maxima. For the cell types investigated, the estimated error rate of the procedure (mistraced cells per trajectory segments obtained) is less than 1%. As initial positions we used centers of clusters obtained by a suitably chosen brightness threshold.

To follow the centrosome and nucleus we tracked the organelles manually in a sequence of images obtained with a 40X objective in both epifluorescence and phase contrast optical modes.

Nuclear positions $x_i(t)$ of various cells i at time points t were determined either automatically or manually, as described above, in every 10 minutes. Nuclear velocity, $v_i(t)$ for cell i at time point t, was calculated from the net displacement during a suitably chosen time interval: $v_i(t) = |x_i(t + \Delta t) - x_i(t)|/\Delta t$. We performed calculations with time lags Δt = 1h and Δt = 20min, resulting in similar relative responses. Unless stated otherwise, the presented velocity data were calculated with the choice of Δt = 1h.

Immunocytochemistry

Immunofluorescent stainings were performed on C6 glioma cells grown on glass coverslips. The cells were fixed with 4% paraformaldehyde in phosphate buffered saline (PBS) for 20 minutes, at room temperature and permeabilized with Triton X-100 (5 min., 0,1% v/v in PBS). Non specific antibody binding was blocked with 5% fetal calf serum (FCS) in PBS at room temperature, for 1 hour. The cultures were incubated overnight at 4°C with antibodies either to vinculin (1:1000 mouse IgG; AbCam), pMLC (1:800 rabbit IgG; AbCam) or γ-tubulin (1:2000, rabbit; Sigma- Aldrich). The actin cytoskeleton was visualized by using phalloidin-biotin conjugate (1:300, Sigma-Aldrich). In some experiments double labeling was performed. The antigens were visualized with the adequate fluorochrome-conjugated secondary antisera (anti-mouse Alexa 488, anti-rabbit Alexa 594 (Invitrogen) in 1:1000 dilutions for 2 h at room temperature. Cell nuclei were labeled with Hoechst 33258 (Sigma-Aldrich). To analyze the immunostained preparations we used either Zeiss Axiovert 200M microscope equipped with ApoTome or a Nikon A1R confocal microscope.

In some experiments, the immunolabeled samples were compared to the last frames of preceding time-lapse recordings. By locating the same cells in both images, we were able to identify the distribution of immunolabeled protein complexes in nucleokinetic cells.

Microprinting

Chemically structured substrates containing 10-20 µm wide stripes permitting and restricting cell attachment were prepared by microcontact printing, one day prior the experiments (Huang et al., 2001; Csucs et al., 2003). Adhesive surfaces were coated with either 40 µg/ml fibronectin or 50 µg/ml poly-L-lysine (Sigma). Blocking of protein/cell attachment was achieved by subsequently covering the surfaces with PLL-PEG, poly-L-lysine-g-poly(ethylene glycol).

Substrate deformation mapping

Flexible polyacrylamide gels were prepared as described by Wang and Pelham (1998). Briefly, 15 µl of acrylamide solution containing 5% acrylamide (Sigma) and 0.06% bis-acrylamide and 1:100 dilution of red fluorescent latex beads (0.5 µm, Sigma) was spread and allowed to polymerize on the surface of 12 mm coverslips activated with silan (Sigma). Fibronectin was covalently coupled to the polyacrylamide gel with photoactivated heterobifunctional reagent sulfo-SANPAH (Pierce). The gel surface was allowed to react with 10 µg/ml fibronectin (Sigma) overnight at room temperature. The Young modulus of the gel with this composition is 1.5×10^4 N/m_2 .

C6 cells were seeded on the fibronectin-covered gel and recorded by automated microscopy in multiple focal planes and both phase contrast and epifluorescence optical modes. At the conclusion of time-lapse recordings cells were removed with trypsinization and additional images recorded the undeformed state of the substrate. Epifluorescence images of the gel surface were selected manually, by subsequent analysis of the image stacks. Bead displacement fields were calculated from a pair of images representing the actual and the undeformed state of the substrate by an automatic cross-correlation analysis (Butler et al., 2002). We employed a subpixel-precision two-stage predictor-corrector method for pattern matching, interrogating in 64 and 16 pixel wide windows (Zamir et al., 2005).

Results

Nuclear motion in elongated radial glia and C6 cells

As reported earlier, C6 cells as well as 3T3 and primary mouse fibroblast cells exhibit oscillatory nuclear movements without substantial cell movements when cultured on micropatterned 20 µm wide fibronectin-coated stripes (Szab´o et al., 2004). The phenomenon can be also observed in spontaneously elongated bipolar C6 cells, a small subpopulation of cells grown on uncoated or uniformly fibronectin-coated tissue culture plastic surfaces. The speed and amplitude of nuclear movement within spontaneously elongated C6 cells is similar to those observed in cells cultured on stripes (Supplementary Fig. S1). Cultured radial glia-like progenitor cells are also often spontaneously bipolar and exhibit oscillatory nuclear movement spontaneously, without micropatterned attachment constrains (Fig. 1a, Movies 1 and 3).

Myosin II inhibition triggers morphological transition with increased nuclear motility

To investigate the role of the actin-myosin system in driving nuclear motility, we exposed cultures of C6 and radial glia-like cells to blebbistatin. Blebbistatin is a widely used drug interfering with normal myosin II function (Kovacs et al., 2004). Administering the drug at 6 µM or higher concentration markedly changes the morphology of both radial glia-like neural progenitors and C6 cells. As Fig. 2 demonstrates, C6 cells cease to spread on the culture surface and exhibit a characteristic bipolar morphology instead. The elongated morphology of radial glia-like cells becomes even more pronounced after blebbistatin treatment, and cells arrange themselves into a sparse multicellular meshwork. C6 cells, when cultured on micropatterned surfaces, also elongate further and spread across the micropatterned stripes (Supplementary Fig. S2). No change can be observed after the administration of the inactive blebbistatin enantiomer (Fig. 2e). The blebbistatin-induced change is reversible, cultures treated with 20 µM blebbistatin resume normal morphology after drug removal (Movie 5).

Surprisingly, cell nuclei become extremely motile in response to blebbistatin (Fig. 1 and Movies 2-5). While blebbistatin-exposed individual radial glia-like or C6 cells show oscillatory nuclear movements, cells attached to other cells move their soma along adjacent cell membranes – a process similar to the astroglia-guided migration of neural progenitor cells. As several nuclear oscillatory cycles can take place without cell divisions, the coupling between cell cycle and nuclear positioning, characteristic for INM, is absent in this in vitro system.

We determined the nucleokinetic response of C6 cells to various doses of blebbistatin. Using an automated tracking software and image sequences obtained from sparse and subconfluent cultures, we traced most nuclei within the cell population. In control cultures most traced nuclei were in well spread cells (Fig. 2c) and typically did not exhibit oscillatory nuclear movement. The population-averaged speed of nuclear movements (including cell motility) is 7.0 ± 0.6 µm/h (n=8 independent recordings). When the concentration of blebbistatin is high enough to trigger the morphological transition shown in Fig. 2, the majority of the nuclei are motile, but at any given moment the nuclei are still unlikely to move with their peak velocity. As Fig. 3 shows, in the 6-50 µM regime blebbistatin increases the population averaged speed of nuclear movements

by 50%. A uniform shift in the distribution of nuclear velocities after blebbistatin treatment suggests that nuclear motility is increased across the whole cell population (Supplementary Fig. S3). The overall increase of nuclear velocities is also demonstrated by radial glia-like cells in Fig. 1 and Movie 3: nuclear movement is further accelerated by blebbistatin even in cells that were bipolar and exhibited rapid nuclear movement before blebbistatin treatment.

Both the change in cell morphology and the increased nuclear motion speed can be partially achieved by Y27632, a ROCK inhibitor, and to a much lesser degree by ML-7, an inhibitor of MLCK (Movie 6). In half of the cell population Y27632 results in a bipolar cell morphology and sustained nuclear motility (Fig. 2f). ML-7 also reduces cell spreading, but the elongated morphology and nuclear movement is not elicited (Fig. 2g). The combination of the two drugs spreads the elongated morphology to a larger population of cells (Fig. 2h), but nuclear movements are not as vigorous as are after the application of blebbistatin or Y27632 alone (Movie 6).

Nuclear motility and centrosome position

In the following, we restrict our investigations to nuclear movements in non-dividing cells and report findings on cultures of C6 cells which are more accessible for experimental manipulations. To visualize centrosomes during nuclear motion, C6 cells were stably transfected with GFP-centrin (Fig. 4a) and recorded with dual-mode phase contrast and epifluorescence time-lapse microscopy. The transfection changed neither the morphology nor the nuclear speed of control and blebbistatintreated cells. The population average speed is 6.9 ± 0.2 µm/h for normal (n=4 independent cultures) while 7.3 ± 1.3 µm/h for transfected cells (n=4 independent cultures, p=0.7).

Centrosomes are readily localized by GFP-centrin fluorescence in the recorded images (Fig. 4b, Movie 7). Most cells exhibited a single centrosome, and we report the behavior of this population. Nuclear and centrosomal movements were compared by intensity profiles, calculated from pixel intensities projected perpendicular to the direction of nuclear movement (Fig. 4c). While the centrosome position is easily projected as a single intensity peak in the epifluorescence image, nuclear positions are visualized using the bright phase contrast halos surrounding the nuclei.

When the nucleus moves, it tends to overtake the centrosome as shown by a typical example in Fig. 4d. This observation is consistent with our previous result (Szabo et al., 2004), when we found that the centrosome tends to stay behind the nucleus in the middle phase of oscillating nuclear movement. As we define front and behind relative to a moving nucleus, when the nucleus changes movement direction and the centrosome remains at the same physical position (Fig. 4c), it still becomes situated in the front. In some instances, however, the centrosome ”jumps”, i.e. is suddenly repositioned to the opposite side of the nucleus as demonstrated in Fig. 4b.

In contrast, when myosin II is blocked, the centrosome is most often found in front of the

moving nucleus as shown in Fig. 5 and Movie 8. Furthermore, while the speed of moving nuclei is substantially increased in blebbistatin-exposed C6 cells, the reversal of nuclear direction takes longer as a typical example in Fig. 5b demonstrates.

After tracing nuclei and centrosomes in image sequences, we calculated the centrosome position relative to the moving nucleus, the speeds of both organelles, and the velocity difference between the two. We analyzed the resulting two dimensional vector data by projecting the vectors to the direction of nuclear movement. The velocity data obtained from cells in which nuclei move faster than 5 µm/h are summarized in Fig. 6. The velocities of the two organelles are very similar, reflecting that in C6 cells the nucleus and the centrosome remain in close proximity.

In untreated cultures (Fig. 6a) the nucleus is on average 30% slower when the centrosome is located in the front. In this configuration the two organelles move with the same speed, and were observed to complete a whole oscillatory half-period. In contrast, when the centrosome is behind the nucleus, it tends to lag further behind. The two organelles, however, were not observed to separate completely.

In cultures treated with 20 µM blebbistatin the centrosome has a stable position in front of the nucleus: if the distance between the organelles is less or more than 5 µm, the centrosome moves faster or slower than the nucleus, respectively (Fig. 6b). Accordingly, as a result of blebbistatin treatment the average position of the centrosome is shifted from behind the nucleus to the front. In these cultures the speed of the nucleus is less effected by the position of the centrosome: the nucleus is on average 15% faster if the centrosome is in the front.

Traction forces

Cell adhesion substrate deformations were visualized during nuclear motion of C6 cells using a suitably modified method of Dembo andWang (1999). We recorded cell cultures in several microscopic fields and subsequently identified cells which spontaneously exhibited a bipolar morphology and oscillating nuclear movement. Bipolar C6 cells exert an order of magnitude weaker traction forces than mesenchymal cells such as fibroblasts or myoblasts do (data not shown). Gel deformations are typically observed around the nucleus and in the vicinity of the leading edge (Fig 7a). The absence of strong and maintained traction forces greatly aids in the detection of slight substrate deformations which accompany nuclear movement. Temporal changes in substrate deformation are in phase with changes in the direction of nuclear motion as the microbead displacements shown in Fig 7b-d demonstrate. The substrate is dragged with the nucleus under most of the cell body. In contrast, stronger forces pull the substrate against the direction of nuclear movement at the leading edge.

Displacements of selected beads were calculated by an automatic, subpixel precision crosscorrelation analysis. The results pooled from different cells (n=6) are summarized in Fig 7e. In accord with the representative bead displacement map in Fig 7a, the largest substrate deformations are localized at the leading edge, where displacements are always directed toward the nucleus. The substrate undergoes smaller deformations in the proximity of the nucleus, where bead displacements are parallel to the direction of nuclear movement. The area where the

substrate is dragged with the nucleus is much larger than the area being pulled at the leading edge towards the nucleus.

Substrate deformations during blebbistatin induced nuclear movement are very weak. Bead displacements at the gel surface were undetectable (being at least an order of magnitude smaller than those obtained from untreated cells), effectively preventing traction force mapping (n=10).

We determined the intracellular distribution of active myosin II during nuclear movements as the myosin II-dependent traction force data suggest a contractile area in front of the nucleus. Several fields of C6 cultures were recorded by time-lapse microscopy. After the conclusion of recordings cultures were fixed immediately and immunolabeled for pMLC, the active phosphorylated regulatory light chain of myosin II. By comparing time-lapse data with immunostained samples, we identified elongated cells which exhibited nuclear movement immediately before fixation. The immunolocalization of pMLC is patchy, with foci associated with the nuclear envelope and cytoskeletal elements (Fig. 7f). Interestingly, the distribution of pMLC is rather symmetric around the nucleus (in some cells the immunofluorescence is slightly more intense at the rear, see Fig. 7g). Thus, our sample of cells with identified nuclear motion and pMLC immunolocalization pattern (n=9) suggest that pMLC does not accumulate in the contractile region between the nucleus and the leading edge.

The roles of actin and microtubule dynamics in nuclear motility

As movement of the nucleus is clearly possible without myosin II activity, we investigated how nuclear movements depend on the normal intracellular dynamics of actin filaments and microtubules. To do so, we exposed C6 cells to microtubule and F-actin stabilizing and destabilizing agents: taxol, vinblastine, jasplakinolide and latrunculin A – both in the presence and absence of blebbistatin (Fig. 8).

The stabilization of F-actin by jasplakinolide slightly reduces nuclear motility either in the presence or absence of blebbistatin. In contrast, a moderate disruption of actin filaments by 50 nM latrunculin A results in a similar behavior seen with the ROCK inhibitor Y-27632, i.e., a transient, hours long, increase in the number of elongated cells with motile nuclei (Movie 9). A more severe disruption of the cytoskeleton by 500 nM Latrunculin A, or by the combination of 20 µM blebbistatin with 50 nM Latrunculin A was found to strongly reduce nuclear movements.

Treatment with vinblastine destroys the cells bipolar morphology. Taxol-treated cells in contrast maintain their bipolar morphology, but the nuclear movements slow down. Nuclear velocity values in Fig. 8g were obtained by automated nuclear tracking which does not discriminate between various types of nuclear motility. Nuclear velocity values obtained after taxol and vinblastine treatments likely reflect random movement of poorly attached cell bodies. In these cells the specific, sustained nuclear movement characteristic of elongated cells is missing (Movie 10). Thus vigorous nuclear movements require the normal intracellular dynamics of both microtubules and F-actin filaments.

Discussion

Cell shape and nuclear movement

Both the in vivo nucleokinesis of migrating neurons and the interkinetic nuclear migration in the developing brain are associated with a highly elongated bipolar cell shape. As we reported earlier (Szabo et al., 2004), on micropatterned stripes C6, 3T3 and primary mouse fibroblast cells that are forced to adopt an elongated bipolar morphology also display a vigorous nuclear movement. Here we report a blebbistatin-induced morphological transition and coincident increased nuclear motion. These observations point to an association between nuclear motility and elongated cell shape.

The reduced cell spreading in our experiments can be resulted by destabilized focal adhesion sites. In elongated cells immunolabeled vinculin forms small foci instead of the extended focal contacts characteristic for well-spread C6 cells (data not shown). The instability of focal contacts can be a consequence of reduced cytoskeletal strain (Balaban et al., 2001). Elongated bipolar cell morphologies emerge due to the reduced cell spreading and the presence of an internal, rigid, microtubule-rich cytoskeleton. The inability of ML-7 to elicit similar changes is probably due to its lower specificity and efficiency (Bain et al., 2003).

Cell polarity

The present as well as our previous report (Szabo et al., 2004) on nuclear motion in spindle-shaped cells show that nucleokinesis is strongly correlated with front/rear polarization of the cell: protrusive activity and membrane ruffling is increased in the direction of nuclear movement. In contrast, the cell body in the opposite direction narrows and partially collapses – resembling the trailing process of a moving cell. Thus, even if cells do not move substantially, nuclear movements are coincident with the characteristic polarized morphologies of motile cells. The sensitivity of the observed nuclear movements to LY294002, a highly selective inhibitor of PI3K, indicates that the well studied phosphatidylinositol-based system for front/rear polarity (Manahan et al., 2004; Gamba et al., 2005) may also be involved in directing nuclear movements irrespective of the activity of myosin II (data not shown). In the following we assume that the direction of nuclear movement is regulated by a biochemical polarity mechanism (Mori et al., 2008).

The positions of the Golgi apparatus and the centrosome are often used, but as we see poor, indicators of cell polarity. These organelles are found in increasingly posterior position in cells cultured on progressively narrower stripes (Pouthas et al., 2008). Although the centrosome of C6 cells is in the front in wound-healing assays (Yamana et al., 2006), in C6 cells constrained to narrow micropatterned stripes the centrosome tends to be behind moving nuclei (Szab´o et al., 2004). The presented results also demonstrate that the position of the centrosome is unlikely to be a mechanistic determinant of front/rear polarity: the polarized morphology is maintained even as the centrosome relocates from the front to the rear (Fig. 4). Furthermore, an oscillating nucleus can reverse motion direction without sudden changes in centrosome position. We

attribute the asymmetric centrosome distribution in spontaneously elongated (or stripe cultured) C6 cells to the observation that fast moving nuclei tend to leave the centrosome behind. Similar behavior was also reported in granule cells (Umeshima et al., 2007).

Cytoskeletal mechanics

The integration of the presented observations into a mechanistic model of nuclear movement is not straightforward. First we discuss possible cytoskeletal processes compatible with the observed traction force pattern, and then discuss the consistency of the resulting model with our experimental results.

Traction and cytoskeletal forces

The myosin-II-dependent traction force distribution of C6 cells is similar to the typical distribution reported for moving fibroblasts (Munevar et al., 2001). The traction force pattern perfectly matches (without observable time delay at our time resolution of 10 minutes) the other observable changes in front/rear polarity, like the dynamics of the leading edge or the direction of nuclear movement.

We argue that the observed contraction in the extracellular substrate, between the nucleus and the leading edge, reflects an intracellular cytoskeletal contraction. Adhesion complexes mechanically link the extracellular environment with local cytoskeletal elements. As according to traction force measurements adhesion complexes at the leading edge and in front of the nucleus are pulled apart by extracellular forces, to maintain mechanical equilibrium, the extracellular forces acting on these complexes must be balanced by intracellular, cytoskeletal contractile forces. Thus, part of the cytoskeleton in front of the moving nucleus is under compression.

Our results together with several other reports (Balaban et al., 2001; Beningo et al., 2006; Even-Ram et al., 2007) establish that traction forces depend on functional myosin II. However, the observed cytoskeletal contractility in front of the nucleus is not a simple consequence of spatially restricted myosin II activity: by immunolabeling the phosphorylated regulatory myosin light chains, we found that pMLC is not localized exclusively between the nucleus and the leading edge. In this respect, C6 cells are similar to other cell types in which myosin II is thought to be more active in the rear than in the front (Lo et al., 2004; Beningo et al., 2006; Even-Ram et al., 2007).

Mechanical model with elastic elements

While the cytoskeletal contraction in front of the nucleus may be still resulted from a spatially restricted active contractile mechanism, distinct from the acto-myosin system, we argue that a simple mechanical model that combines active and passive cytoskeletal elements is compatible with all our observations. The classification of cytoskeletal elements into actively contractile (acto-myosin) and passive, compressed elements which are in mechanical equilibrium was first suggested in the tensegrity model (Ingber, 2006). We apply this concept to construct a one dimensional ”cartoon” model, which consist of a long-range, active, contractile element and a

chain of shorter passive elements (Fig. 9a). We assume that the active element (similar to an acto-myosin stress cable) is capable of generating a constant contractile force irrespective of its length. The force exerted by a passive element is determined by its deformation (change in length). For simplicity we further assume that the passive and active elements only interact at the two ends of the linear chain of passive elements. Finally, the structure is coupled to an elastic environment.

If the passive elements are elastic, one can calculate each force by requiring mechanical equilibrium throughout the structure (Fig. 9b). In this system the contraction of the active element is balanced by the compression of passive elements, and by forces exerted by the environment. Thus, the amount of compression at any given location depends not only on the contractile force, but also on the stiffness distribution of the passive elements within the entire structure. As the configuration in Fig. 9b demonstrates, a compliant passive element can create a local compression which is also mirrored in the deformation of the environment. In this model the location of the active element is irrelevant as long as it is capable to compress the entire structure.

Mechanical model with viscoelastic elements

To account for a sustained nuclear motion, we extend the caricature model so that its passive elements are capable to relax mechanical stress. The viscoelastic behavior of the cytoskeleton is well documented (Forgacs et al., 1998; Balland et al., 2006) and it is a direct consequence of the cell's ability to depolymerize and remodel cytoskeletal filaments or microtubules. We argue that during a several hour time period, which is needed for the nucleus to traverse the cell, the cytoskeleton remodels in such a way that intrinsic stresses are eliminated. In other words, the nucleus will not move back to one of its previous positions even if we suddenly turned off the active driving force. Thus we model the long-term behavior of the cytoskeleton as a Maxwell fluid, and its flow properties are characterized by viscosity values μ (Fig. 9c). We consider substantial cytoskeletal remodeling in front of the nucleus, and between the moving bulk of the cytoskeleton and the environment. The latter is needed as at any given moment the cell organelles and the extracellular environment are mechanically coupled through the cytoskeleton, therefore any relative movement of these objects requires a "clutch". The relaxation of the shear stress may take place within the cytoskeleton or at the adhesion sites as its molecular components are turned over (Kuusela and Alt, 2009; Fournier et al., 2010). In this respect the leading edge is special, where a combination of processes maintains a stable anchor region even as individual adhesion sites may turn over.

The forces in a steady state configuration can be calculated by requiring mechanical equilibrium for each element, and the co-movement (same velocity v) of the moving elements. In this simple model the traction forces under the "cell body" are $v\mu_1$, while at the leading edge it is $3v\mu_1$. From the force balance at the leading edge we can obtain

$$v(3\mu_1 + \mu_2) = F_{active} \ , \qquad (1)$$

thus the bulk speed of the cytoskeleton is determined by both the magnitude of the contractile force and a viscosity-like quantities which describe the ability of the cytoskeleton to remodel and dissipate mechanical stresses.

Comparison with empirical results

This simple mechanical model can help us interpret the somewhat puzzling observation that nuclear motion speeds up after disabling a force generation mechanism. Our results suggest that there are at least two parallel mechanisms able to drive the nucleus. As nuclei can move in the presence of blebbistatin, one mechanism does not utilize myosin II. Although myosin II is dispensable to nuclear motion, the reversed centrosome position indicates that a different mechanical state moves the nucleus when myosin II is inactive. Based on the above model (Fig 9c) it is also reasonable to assume that acto-myosin contraction, when present in C6 cells, also contributes to move the cytoskeleton and organelles anchored to it (Fig. 9d). Thus, we assume that active forces are generated by two parallel mechanisms as

$$F_{active} = F_1 + [myo]F_2 \quad (2)$$

where [myo] denotes the average active myosin II concentration, and F_1 denotes the myosin-independent force. While the absence of traction forces lead to a disassembly of adhesion sites and stress cables, an increasing amount of active myosin II is likely to increase the cytoskeletal viscosity (Martens and Radmacher, 2008):

$$\mu = \mu_0 + k[myo]. \quad (3)$$

Combining (1) with (2) and (3) and lumping the various viscosity values in μ we obtain

$$v \sim (F_1 + [myo]F_2)/(\mu = \mu_0 + k[myo]) \quad (4)$$

for the bulk cytoskeletal speed *v*. Expression (4) is a monotonically decreasing function of the active myosin concentration [myo] if μ_0 is small enough. Thus, our simple caricature model is consistent with the finding that blebbistatin increases nuclear motility.

Moreover, the results obtained with drugs perturbing cytoskeletal dynamics are also consistent with the view that for sustained nuclear movement cytoskeletal remodeling is needed, and the speed is determined by the balance of driving forces and cytoskeletal resistance to remodeling. As the cytoskeleton is required for a large number of cellular processes, a substantial cytoskeletal disruption (e.g., with high doses of latrunculin A) alters not only the intracellular mechanical balance but the fundamental cell functions as well – therefore observations under such conditions are not as conclusive as experiments resulting only in moderate alterations in the cytoskeleton.

Myosin-independent nuclear motility

In the absence of myosin II activity the nucleus is likely to be pulled by microtubule-associated motors as in such cases the centrosome tends to move before the nucleus (Fig. 9e). Myosin IIA-deficient human fibroblasts were recently shown to display substantially increased cell

movement which was dependent on the microtubule motor kinesin Eg5 (Even-Ram et al., 2007). While we could not detect reduced nuclear motility in blebbistatin exposed C6 cells by further treatment with 50 μM monastrol, an Eg5-specific inhibitor, (data not shown) – other microtubule associated motors, such as cytoplasmic dyneins are candidates for being involved in the process.

Considering both the myosin II dependent and independent mechanisms, we suggest that microtubule-associated forces act at the centrosome. Thus, we propose that in cells where the centrosome is in front the nucleus is mainly driven by microtubule related forces. Conversely, when the centrosome is lagging behind, the nucleus can be moved by contractile forces independent of the centrosome, such as exerted by myosin II (Munevar et al., 2001; Pan et al., 2009). The slower speed of the centrosome may reflect a larger intracellular resistance to move a large part of the microtubular system: the effective viscosity for the centrosome can be larger than that for the nucleus. In a formal model we suggest that the parameters μ and F_{active} can be distinct for the organelles, and these differences are responsible for the altered location of the centrosome during nucleokinesis. This mechanism appears to be relevant for neuronal cell migration in a 3D environment (Doyle et al., 2009), which was found to be myosin II and microtubule dependent with a posterior centrosome location.

Acknowledgements

We are grateful to Dr. Tamás Vicsek for his help in fluorescent time-lapse imaging and following consultations. We thank Dr. Emilia Madarász for her ideas and helpful comments on the manusript. We thank Dr. Salisbury for providing the GFP-centrin plasmid. We thank Zsófia Jurányi and Gergely Nagy for their help in image analysis. László Barna, the Nikon Microscopy Center at IEM, Nikon Austria GmbH and Auro-Science Consulting Ltd kindly provided microscopy support. This work was supported by Hungarian Research Fund grants NKFP 3A/0005/2002 (to Dr. Vicsek), OTKA F49795 (to B. Sz.), OTKA T47055 (to A. C.) and the ELTE RET grant of the Hungarian National Office for Research and Technology.

References

Ahringer, J. (2003). Control of cell polarity and mitotic spindle positioning in animal cells. Curr Opin Cell Biol 15, 73–81.

Bain, J., McLauchlan, H., Elliott, M. and Cohen, P. (2003). The specificities of protein kinase inhibitors: an update. Biochem J. 371, 199–204.

Balaban, N. Q., Schwarz, U. S., Riveline, D., Goichberg, P., Tzur, G., Sabanay, I., Mahalu, D., Safran, S., Bershadsky, A., Addadi, L. et al. (2001). Force and focal adhesion assembly: a close relationship studied using elastic micropatterned substrates. Nat Cell Biol 3, 466–472.

Balland, M., Desprat, N., Icard, D., Frol, S., Asnacios, A., Browaeys, J., Hnon, S. and Gallet, F. (2006). Power laws in microrheology experiments on living cells: Comparative analysis and modeling. Phys Rev E Stat Nonlin Soft Matter Phys 74, 021911.

Beningo, K. A., Hamao, K., Dembo, M., Wang, Y.-L. and Hosoya, H. (2006). Traction forces of fibroblasts are regulated by the rho-dependent kinase but not by the myosin light chain kinase. Arch Biochem Biophys 456, 224–231.

Brito, D. A., Strauss, J., Magidson, V., Tikhonenko, I., Khodjakov, A. and Koonce, M. P. (2005). Pushing forces drive the comet-like motility of microtubule arrays in dictyostelium. Mol Biol Cell 16, 3334–3340.

Butler, J. P., Tolic-Norrelykke, I. M., Fabry, B. and Fredberg, J. J. (2002). Traction fields, moments, and strain energy that cells exert on their surroundings. Am J Physiol Cell Physiol 282, C595–C605.

Cowan, C. R. and Hyman, A. A. (2004). Centrosomes direct cell polarity independently of microtubule assembly in C. elegans embryos. Nature 431, 92–96.

Cs´ucs, G., Michel, G. R., Lussi, J.W., Textor, M. and Danuser, G. (2003). Microcontact printing of novel co-polymers in combination with proteins for cell-biological applications. Biomaterials 24, 1713–20.

Czirok, A., Rupp, P., Rongish, B. and Little, C. (2002). Multi-field 3D scanning light microscopy of early embryogenesis. J Microsc. 206, 209–17.

Danowski, B. A., Khodjakov, A. and Wadsworth, P. (2001). Centrosome behavior in motile HGF-treated ptk(2) cells expressing GFP-gamma tubulin. Cell. Motil. Cytoskeleton 50, 59–68.

D'Assoro, A. B., Stivala, F., Barrett, S., Ferrigno, G. and Salisbury, J. L. (2001). GFP-centrin as a marker for centriole dynamics in the human breast cancer cell line mcf-7. Ital J Anat Embryol 106, 103–110.

de Anda, F. C., Pollarolo, G., Silva, J. S. D., Camoletto, P. G., Feiguin, F. and Dotti, C. G. (2005). Centrosome localization determines neuronal polarity. Nature 436, 704–8.

Dembo, M. andWang, Y. L. (1999). Stresses at the cell-to-substrate interface during locomotion of fibroblasts. Biophys J 76, 2307–2316.

Ding, D.-Q., Chikashige, Y., Haraguchi, T. and Hiraoka, Y. (1998). Oscillatory nuclear movement in fission yeast meiotic prophase is driven by astral microtubules, as revealed by continuous observation of chromosomes and microtubules in living cells. J. Cell Sci. 111, 701–712.

Doyle, A. D., Wang, F. W., Maatsumoto, K. and Yamada, K. M. (2009). One-dimensional topography underlies three-dimensional fibrillar cell migration. JCB 184, 481–90.

Even-Ram, S., Doyle, A. D., Conti,M. A., Matsumoto, K., Adelstein, R. S. and Yamada, K. M. (2007). Myosin IIa regulates cell motility and actomyosin-microtubule crosstalk. Nat Cell Biol 9, 299–309.

Forgacs, G., Foty, R. A., Shafrir, Y. and Steinberg, M. S. (1998). Viscoelastic properties of living embryonic tissues: a quantitative study. Biophys J 74, 2227–2234.

Fournier, M. F., Sauser, R., Ambrosi, D., Meister, J.-J. and Verkhovsky, A. B. (2010). Force transmission in migrating cells. J Cell Biol 188, 287–297.

Frade, J. M. (2002). Interkinetic nuclear movement in the vertebrate neuroepithelium: encounters with an old acquaintance. Prog. Brain Res. 136, 67–71.

Friedlander, D. R., Brittis, P. A., Sakurai, T., Shif, B., Wirchansky, W., Fishell, G. and Grumet, M. (1998). Generation of a radial-like glial cell line. J Neurobiol 37, 291–304.

Gamba, A., de Candia, A., Talia, S. D., Coniglio, A., Bussolino, F. and Serini, G. (2005). Diffusion-limited phase separation in eukaryotic chemotaxis. Proc Natl Acad Sci U S A 102, 16927–16932.

Gönczy, P., Echeverri, C., Oegema, K., Coulson, A., Jones, S. J., Copley, R. R., Duperon, J., Oegema, J., Brehm, M., Cassin, E. et al. (2000). Functional genomic analysis of cell division in C. elegans using RNAi of genes on chromosome III. Nature 408, 331–336.

Holly, T. E., Dogterom, M., Yurke, B. and Leibler, S. (1997). Assembly and positioning of microtubule asters in microfabricated chambers. PNAS 96, 6228–31.

Huang, N.-P., Michel, R., Vörös, J., Textor, M., Hofer, R., Rossi, A., Elbert, D. L., Hubbell, J. A. and Spencer, N. D. (2001). Poly(l-lysine)-g-poly(ethylene glycol) layers on metal oxide surfaces: Surface-analytical characterization and resistance to serum and fibrinogen adsorption. Langmuir 17, 489–98.

Ingber, D. E. (2006). Cellular mechanotransduction: putting all the pieces together again. FASEB J 20, 811–827.

Kole, T. P., Tseng, Y., Jiang, I., Katz, J. L. and Wirtz, D. (2005). Intracellular mechanics of migrating fibroblasts. Mol Biol Cell 16, 328–338.

Kovács, M., Tóth, J., Hetényi, C.,Málnási-Csizmadia, A. and Sellers, J. R. (2004). Mechanism of blebbistatin inhibition of myosin II. J Biol Chem 279, 35557–35563.

Kriegstein, A. and Alvarez-Buylla, A. (2009). The glial nature of embryonic and adult neural stem cells. Annu Rev Neurosci 32, 149–84.

Kuusela, E. and Alt, W. (2009). Continuum model of cell adhesion and migration. J Math Biol 58, 135–161.

Lo, C.-M., Buxton, D. B., Chua, G. C. H., Dembo, M., Adelstein, R. S. and Wang, Y.-L. (2004). Nonmuscle myosin IIb is involved in the guidance of fibroblast migration. Mol Biol Cell 15, 982–989.

Manahan, C. L., Iglesias, P. A., Long, Y. and Devreotes, P. N. (2004). Chemoattractant signaling in Dictyostelium discoideum. Annu Rev Cell Dev Biol 20, 223–253.

Marko, K., Ligeti, M., Mezo, G., Mihala, N., Kutnyanszky, E., Kiss, E., Hudecz, F. and Madarasz, E. (2008). A novel synthetic peptide polymer with cyclic RGD motifs supports serum free attachment of anchorage-dependent cells. Bioconjug Chem 19, 1757–66.

Martens, J. C. and Radmacher, M. (2008). Softening of the actin cytoskeleton by inhibition of myosin II. Pflugers Arch 456, 95–100.

Mori, Y., Jilkine, A. and Edelstein-Keshet, L. (2008). Wave-pinning and cell polarity from a bistable reaction-diffusion system. Biophys J 94, 3684–3697.

Morris, N. R. (2000). Nuclear migration: from fungi to the mammalian brain. J. Cell Biol. 148, 1097–1101.

Morris, N. R. (2003). Nuclear positioning: the means is at the ends. Curr. Opin. Cell. Biol. 15, 54–59.

Mosley-Bishop, K. L., Li, Q., Patterson, L. and Fischer, J. A. (1999). Molecular analysis of the klarsicht gene and its role in nuclear migration within differentiating cells of the drosophila eye. Curr Biol 9, 1211–1220.

Munevar, S., Wang, Y. and Dembo, M. (2001). Traction force microscopy of migrating normal and hüras transformed 3T3 fibroblasts. Biophys J 80, 1744–1757.

Murciano, A., Zamora, J., Lopez-Sanchez, J. and Frade, J. M. (2002). Interkinetic nuclear movement may provide spatial clues to the regulation of neurogenesis. Mol. and Cell. Neuroscience 21, 285–300.

Niu, M. Y., Mills, J. C. and Nachmias, V. T. (1997). Development of polarity in human erythroleukemia cells: roles of membrane ruffling and the centrosome. Cell. Motil. Cytoskeleton 36, 203–15.

Pan, Z., Ghosh, K., Liu, Y., Clark, R. A. F. and Rafailovich, M. H. (2009). Traction stresses and translational distortion of the nucleus during fibroblast migration on a physiologically relevant ECM mimic. Biophys J 96, 4286–4298.

Pollard, S. and Conti, L. (2007). Investigating radial glia in vitro. Progress in neurobiology 83, 53–67.

Pouthas, F., Girard, P., Lecaudey, V., Ly, T. B. N., Gilmour, D., Boulin, C., Pepperkok, R. and Reynaud, E. G. (2008). In migrating cells, the golgi complex and the position of the centrosome depend on geometrical constraints of the substratum. JCS 121, 2406–14.

Robinson, J. T., Wojcik, E. J., Sanders, M. A., McGrail, M. and Hays, T. S. (1999). Cytoplasmic dynein is required for the nuclear attachment and migration of centrosomes during mitosis in drosophila. J Cell Biol 146, 597–608.

Rowat, A. C., Lammerding, J., Herrmann, H. and Aebi, U. (2008). Towards an integrated understanding of the structure and mechanics of the cell nucleus. Bioessays 30, 226–236.

Schaar, B. T. and McConnell, S. K. (2005). Cytoskeletal coordination during neuronal migration. PNAS 102, 13652–57.

Schenk, J., Wilsch-Brauninger, M., Calegari, F. and Huttner, W. B. (2009). Myosin ii is required for interkinetic nuclear migration of neural progenitors. PNAS 106, 16487–92.

Shu, T., Ayala, R., Nguyen, M.-D., Xie, Z., Gleeson, J. G. and Tsai, L.-H. (2004). Ndel1 operates is a common pathway with Lis1 and cytoplasmic dynein to regulate cortical neuronal positioning. Neuron 44, 263–77.

Solecki, D. J., Model, L., Gaetz, J., Kapoor, T. M. and Hatten, M. E. (2004). Par6alpha signaling controls glial-guided neuronal migration. Nat. Neurosci. 7, 1195–1203.

Solecki, D. J., Trivedi, N., Govek, E. E., Kerekes, R. A., Gleason, S. S. and Hatten, M. E. (2009). Myosin II motors and F-actin dynamics drive the coordinated movement of the centrosome and soma during CNS glial-guided neuronal migration. Neuron 63, 63–80.

Szabó, B., Környei, Z., Zách, J., Selmeczi, D., Csúcs, G., Czirók, A. and Vicsek, T. (2004). Auto-reverse nuclear migration in bipolar mammalian cells on micropatterned surfaces. Cell Motil. Cytoskeleton 59, 38–49.

Tran, P. T., Marsh, L., Doye, V., Inoue, S. and Chang, F. (2001). A mechanism for nuclear positioning in fission yeast based on microtubule pushing. J. Cell Biol. 153, 397–411.

Tsai, J.-W., Bremner, K. H. and Vallee, R. B. (2007). Dual subcellular roles for lis1 and dynein in radial neuronal migration in live brain tissue. Nat. Neurosci. 10, 970–79.

Tsai, J.-W., Chen, Y., Kriegstein, A. R. and Vallee, R. B. (2005). Lis1 RNA interference blocks neural stem cell division, morphogenesis, and motility at multiple stages. J. Cell Biol. 170, 935–45.

Tsai, J.-W., Lian, W.-N., Kemal, S., Kriegstein, A. R. and Vallee, R. B. (2010). Kinesin 3 and cytoplasmic dynein mediate interkinetic nuclear migration in neural stem cells. Nat Neurosci 13, 1463–1471.

Tsai, L.-H. and Gleeson, G. (2005). Nucleokinesis in neuronal migration. Neuron 46, 383–88.

Umeshima, H., Hirano, T. and Kengaku, M. (2007). Microtubule-based nuclear movement occurs independently of centrosome positioning in migrating neurons. PNAS 104, 16182–87.

Wang, Y. L. and Pelham, R. J. (1998). Preparation of a flexible, porous polyacrylamide substrate for mechanical studies of cultured cells. Methods Enzymol 298, 489–496.

Whited, J. L., Cassell, A., Brouillette, M. and Garrity, P. (2004). Dynactin is required to maintain nuclear position within postmitotic drosophila photoreceptor neurons. Development 131, 4677–86.

Wittmann, T. and Waterman-Storer, C. M. (2001). Cell motility: can rho GTPases and microtubules point the way? J Cell Sci 114, 3795–3803.

Yamana, N., Arakawa, Y., Nishino, T., Kurokawa, K., Tanji, M., Itoh, R. E., Monypenny, J., Ishizaki, T., Bito, H., Nozaki, K. et al. (2006). The rho-mdia1 pathway regulates cell polarity and focal adhesion turnover in migrating cells through mobilizing apc and c-src. Molecular and Cellular Biology 26, 6844–58.

Yvon, A. M.,Walker, J.W., Danowski, B., Fagerstrom, C., Khodjakov, A. and Wadsworth, P. (2002). Centrosome reorientation in wound-edge cells is cell type specific. Mol. Biol. Cell. 13, 1871–80.

Zamir, E. A., Czirok, A., Rongish, B. J. and Little, C. D. (2005). A digital image-based method for computational tissue fate mapping during early avian morphogenesis. Ann Biomed Eng 33, 854–865.

Zhang, X., Lei, K., Yuan, X., Wu, X., Zhuang, Y., Xu, T., Xu, R. and Han, M. (2009). Sun1/2 and syne/nesprin-1/2 complexes connect centrosome to the nucleus during neurogenesis and neuronal migration in mice. Neuron 64, 147–9.

Figure captions

Figure 1: Radial glia-like cells engage in an oscillatory nuclear motion, similar to INM. Image sequences, with a rate of 10 min/frame, depict an untreated (a) and a blebbistatin-treated (20 µM) cell (b). The nucleus of most blebbistatin treated radial glia-like cells becomes extremely motile. Phase contrast images, scale bars: 50 µm. See also Movies 1 and 2.

Figure 2: Blebbistatin induced morphology change in radial glia-like (a,b) and C6 cells (c,d). When compared to control (DMSO treated) cells (a, c), 20 µM blebbistatin (b, d) induces a bipolar morphology: most cells exhibit two extremely narrow processes with the soma in between. Both cell types arrange into a sparse meshwork. e: The inactive blebbistatin enantiomer, shown here also at 20µM concentration, is indistinguishable from untreated cells. f: 40 µM ROCK inhibitor Y27632 induces a morphology and motility switch similar to that of blebbistatin. g: 20 µM ML7, an MLCK inhibitor, reduces cell spreading, but does not result in bipolar morphologies or fast moving nuclei. h: The combined treatment with ML7 and Y27632 results in bipolar morphologies in a larger population of cells. Phase contrast images, scale bar: 100µm. See also Movies 3-6.

Figure 3: Normalized speed of nucleus movements in C6 cells as a function of blebbistatin concentration. Myosin II inhibition provokes increased nuclear motility even at relatively high concentration of blebbistatin. The population average speed of nuclei in blebbistatin treated cultures were normalized to similar averages obtained in parallel control cultures. The average nuclear speed in control cultures is 7 ± 0.6 µm/h (n=9 fields). Error bars represent SEM, calculated from independent microscopic fields (n=3 for 1 and 3 µM; n=4 for 6 µM; n=9 for 20 µM; and n=2 for 50 µM). In two-sided t-tests significance values $p < 0.05$ were considered significant and marked by asterisks. Each analyzed field contained at least 100 tracked nuclei and more than 5000 nucleus positions.

Figure 4: Centrosome position during nuclear movement in C6 cells. a: The centrosome is visualized by GFP-centrin epifluorescence (green) in a typical cluster of transfected C6 cells. Immunostaining with anti-centrin antibodies (red) gives exact co-localization (yellow) at the resolution of the 100X oil immersion objective. Nuclei are stained with a Hoechst reagent (blue). Insets show the red (top) and green (bottom) channels inverted for better contrast. b: A GFP-centrin transfected C6 cell, cultured on a 20 µm wide micropatterned fibronectincoated stripe, is shown in consecutive time points. Grayscale phase contrast and green fluorescence time-lapse images were superimposed to show the centrosome position (see also Movie 7). Red arrows point to the centrosome. Approximate edges of the bright halo (a phase contrast effect) surrounding the nucleus is marked by a red and a yellow asterisk. The image sequence depicts a reversal of nucleus direction. During this particular event, the centrosome moved suddenly relative to the nucleus (between frames taken at 60 and 70 minutes). c: Centrosome position during several nuclear oscillations. Intensity profiles were obtained by projecting the brightest pixels in the direction perpendicular to the long cell axis. Thus, a horizontal line of panel c corresponds to a single time-lapse frame, like those shown in panel b. Light gray areas reveal the position of the phase contrast halo surrounding the nucleus, green dots mark the centrosome. Frames shown in panel b correspond to the sequence between the red lines. Red and yellow

asterisks label the same locations as in the frame at 40 min in panel b. Some, but not all nuclear turns contain a sudden relocation of the centrosome, similar to the event depicted in panel b. d: The nucleus tends to overtake the centrosome between the turns. Intensity profiles, similar to panel c, are depicting nuclear and centrosome movement between two nuclear direction reversals. The approximate leading and trailing nucleus boundaries are marked with red dotted lines. While the centrosome initially is at the front of the nucleus, it lags behind: the upper red bracket is longer than the lower one.

Figure 5: Centrosome position during blebbistatin-induced nuclear movement in C6 cells. a: The centrosome visualized by GFP-centrin epifluorescence in a typical transfected C6 cell treated with 20 µM blebbistatin. Grayscale phase contrast and green fluorescence time-lapse images were superimposed to show the centrosome position (see also Movie 8). Red arrows point to the centrosome. Approximate edges of the bright halo (a phase contrast effect) surrounding the nucleus is marked by a red and yellow asterisk. b: Centrosome position during nuclear movement, plotted as in Fig 4c. Frames shown in panel a correspond to the area between the red lines. Red and yellow asterisks mark the same locations as in panel a. The centrosome tends to be in front of a moving nucleus. We did not observe rapid alterations in the direction of blebbistatin-induced nuclear motility.

Figure 6: Average organelle speeds as a function of centrosome position, in untreated (a) and 20 µM blebbistatin-treated cultures (b). Speed of the nucleus (blue) and the centrosome (green) are plotted together with their relative speed (red). The presented data includes only cells in which the nucleus moved faster than 5 µm/h and where the centrosome was detectable. At least 160 data points were binned and averaged based on the relative position of the centrosome along the cell axis. Speed and position values were obtained by projecting the two dimensional vector quantities to the direction of nuclear movement. Speed values reflect instantaneous movements, calculated from displacements during 10 minutes. The more compact nucleus and cell body of blebbistatin-treated cells is reflected by the smaller scale of position differences in panel (b). The velocity of the two organelles are very similar, a consequence of the fact that in C6 cells the nucleus and the centrosome remain in close proximity. Error bars represent SEM. Direction of nuclear movement is indicated by horizontal red arrows.

Figure 7: Substrate deformations indicate a contraction between the leading edge and the nucleus during nuclear movement in spontaneously elongated C6 cells. a: Bead positions (green) during nuclear movement of a cell outlined with dotted line, superimposed upon the stressfree configuration obtained by trypsin treatment (red). Substantial bead displacements, characterized by the lack of colocalization of green and red colors, are visible at the leading edge (large white arrow). Displacements of smaller magnitude characterize the area surrounding the nucleus (small white arrows). Beads far from the cell show no displacement (circles). The direction of nuclear movement is indicated by the red arrow. Bead aggregates yield larger fluorescent blobs. b-d: Intensity profiles, obtained as in Fig. 4c, of a typical oscillating cell show that bead displacements (b) change in synchrony with the direction of nuclear movements (c). The nucleus appears as a bright stripe and horizontal dotted lines are visual guides, denoting phases of oscillating nuclear movement. The vertical red and green lines, separated by 10 µm, mark the same location in both (b) and (c). Arrowheads point to bead displacements. Beads far from the cell show no displacements during the same time interval (d). e: Bead displacements, pooled

from n=6 cells, are plotted against their relative position along the front/rear axis of the cell. The zero and unit abscissa values denote the nucleus and the leading edge, respectively. Positive displacements are parallel to the direction of cell movement, indicated by the red arrow. f: Immunocytochemical localization of pMLC (red) in C6 cells, superimposed upon images of phalloidin-labeled filamentous actin (green) and a Hoechst nuclear stain (blue). The distribution of pMLC labeled foci is quite symmetric in both well spread and elongated cells. The vicinity of the nucleus is the source of the most intense pMLC immunofluorescence. g: Immunocytochemical localization of pMLC (red) superimposed upon images of vinculin immunofluorescence (green) and a Hoechst nuclear stain (blue). A C6 cell is shown in which the nucleus moved intensively in the direction marked by the red arrow. pMLC can be found both in the front and in the rear of the nucleus. The viculin immunostaining indicates the presence of scattered small adhesion sites instead of extended focal contacts characteristic of fully spread C6 cells in culture.

Figure 8: The role of normal cytoskeletal turnover in nuclear motility. C6 cells are exposed to microtubule and F-actin stabilizing and destabilizing agents: taxol, vinblastin, jasplakinolide and latrunculin A. Characteristic cell morphologies are shown for 100 nM jasplakinolide (a), together with 20 µM blebbistatin (b); 50 nM latrunculin A (c), together with 20 µM blebbistatin (d); and 20 nM vinblastine (e) and 30 nM taxol (f) together with 20 µM blebbistatin. g: Population and time-averaged nuclear speeds, obtained by automatic tracking, are compared to that of untreated cultures at 7 _ 0:6 µm/h (green lines). Blebbistatin concentration is 20 µM. The labels jaspla, latA and vbl indicate jasplakinolide, latrunculin A and vinblastine, respectively. Error bars represent standard error of the mean. See also Movies 9 and 10.

Figure 9: Schematic model of cytoskeletal dynamics during nuclear movements. We consider a system of an active contractile element (red spring) and a chain of passive elements (black springs) attached to an elastic environment (blue objects). a: If the active element is turned off, no forces are present in the system. b: When the active element contracts, this force is balanced by the compression of the passive elements and deformation of the environment. Forces exerted by the elements are represented by arrows. Compression and tension of the elements is indicated by yellow and green vectors, respectively. We assume that the passive element in the front (the spring drawn with a thinner line) is more compliant, which creates an uneven compression pattern and a matching asymmetry in forces within the environment (forces exerted by the blue springs). c: To accommodate a sustained movement of a large part of the structure (red arrows) we introduce elements, represented by dashpots, which can dissipate mechanical stress. The spring and dashpot in a serial arrangement models the cytoskeleton as a viscoelastic Maxwell fluid. The dissipative elements couple the speed of movement and the force exerted upon the element, the conversion factors are marked as μ_1 and μ_2. Forces can be established by requiring mechanical equilibrium and the co-movement of the elements marked by red arrows. d: The elements shown in panel c are represented within a cartoon of a contractile cell. Traction forces exerted by the cell are marked as vectors and matched with the corresponding forces by dashed gray lines. The passive cytoskeleton is represented as a hatch pattern. Areas where we assume intensive dissipation of mechanical tension (remodeling) are marked yellow and matched by the corresponding dashpots with gray dashed lines. The active contractile elements are shown as green lines (actin filaments) and red disks (myosin II motors). e: In the absence of myosin II activity, the cytoskeleton is more compliant, and we envision a microtubule-based mechanism to

move the nucleus: Cortical motors (magenta) pull the astral microtubules (cyan) and the centrosome (green disk), which in turn, is linked (thick black line) to the nucleus. This mechanism may operate in parallel with the myosin II dependent contractility shown in panel d.

Supplemental Fig S1: Elongated morphology and oscillatory nuclear movements in C6 cells. Some cells spontaneously display an elongated morphology, even in a homogeneous tissue culture environment (a). Cells cultured on 20 µm wide fibronectin coated stripes are constrained into an elongated morphology (b). Nuclear movements are visualized by projecting the brightest pixel intensities perpendicular to the long cell axis, for each time-lapse frame resulting in the horizontal lines of the image. The phase contrast halo surrounding the cell soma traces nuclear movements as a bright curve in these images. Oscillatory nuclear movement, of similar magnitude and speed is evident both in a spontaneously elonged cell (c) or in an attachment-constrained cell (d). The images show a 50 µm X 200 µm large area, the brackets indicate 4 hour long timespans in panels c and d.

Supplemental Fig S2: Blebbistatin treated cells ignore adhesion constraints. C6 cells do not spread across the PLL-PEG-coated stripes and assume an elongated morphology (a). Six hours later, in the presence of 6 µM blebbistatin the cells can spread across the PLL-PEG stripes. The same microscopic field, 0.9 mm wide, is shown in both panels. The microprinted substrate consists of alternating PLL-PEG and fibronectin coated stripes, both 20 µm wide.

Supplemental Fig S3: Blebbistatin increases nuclear movements across the whole cell population of C6 cells. The cumulative distribution function of nuclear velocities is shown, giving the probability that a randomly chosen nuclear speed value will be larger than the value at the abscissa. Each graph includes the whole automatically tracked cell population of the microscopic field of view, and all possible time points where a nuclear speed was determined. Black and red curves correspond to data obtained from control and 20 µM blebbistatin treated cultures, respectively.

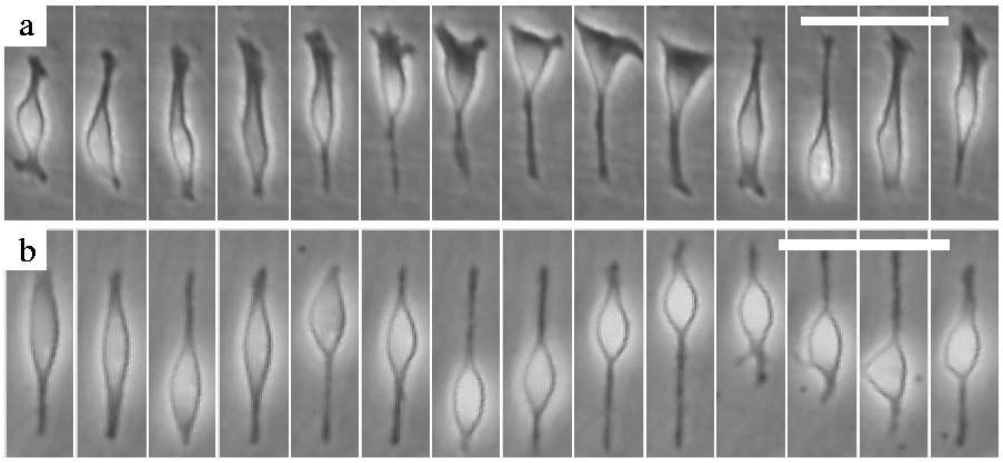

Fig. 1. Radial glia-like cells engage in an oscillatory nuclear motion, similar to INM. Image sequences, with a rate of 10 min/frame, depict an untreated (a) and a blebbistatin-treated (20 μM) cell (b). The nucleus of most blebbistatin treated radial glia-like cells becomes extremely motile. Phase contrast images, scale bars: 50 μm. See also supplementary videos 1 and 2.
318x147mm (72 x 72 DPI)

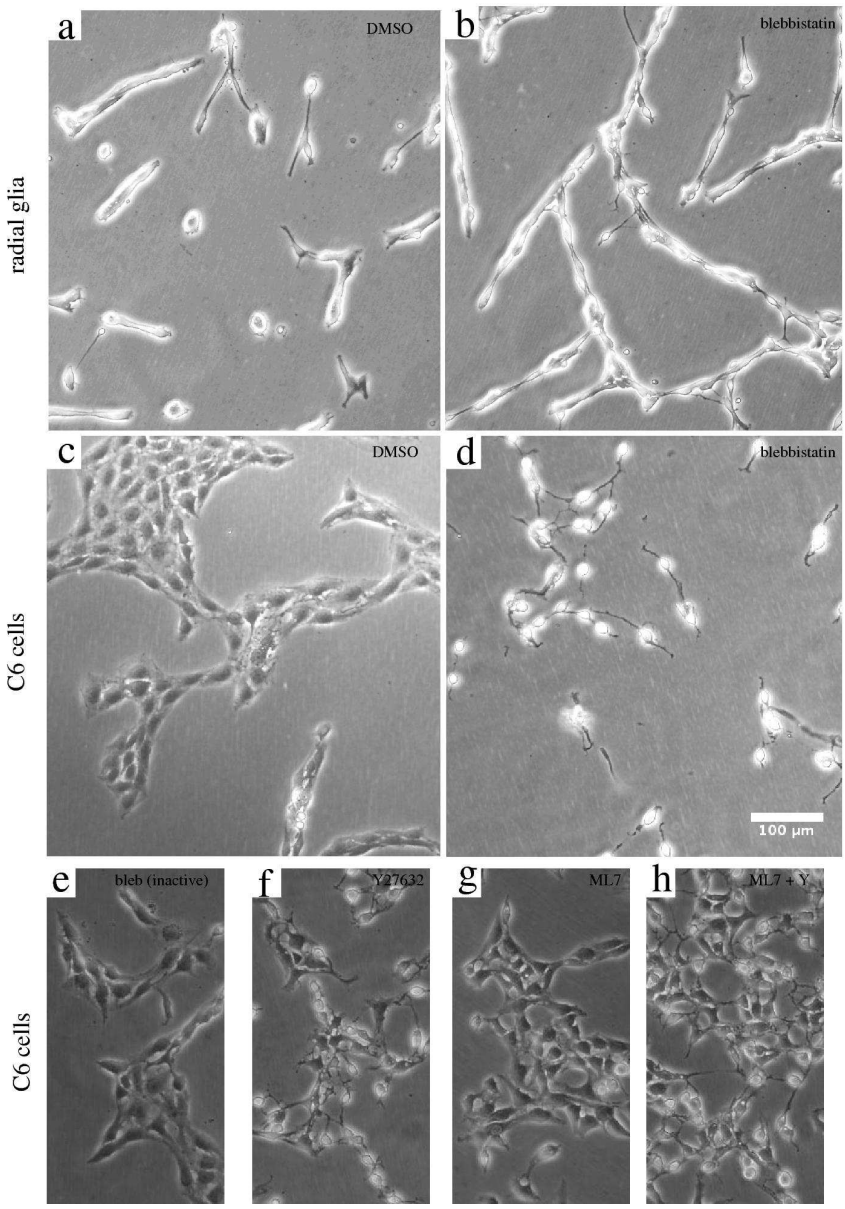

Blebbistatin induced morphology change in radial glia-like (a,b) and C6 cells (c,d). When compared to control (DMSO treated) cells (a, c), 20 μM blebbistatin (b, d) induces a bipolar morphology: most cells exhibit two extremely narrow processes with the soma in between. Both cell types arrange into a sparse meshwork. The inactive blebbistatin enantiomer, shown here also at 20μM, is indistinguishable from untreated cells (e). The ROCK inhibitor Y27632 induces a morphology and motility switch similar to that of blebbistatin. In panel (f) the response is shown for 40 μM Y27632. 20 μM ML7, an MLCK inhibitor, reduces cell spreading, but does not result in bipolar morphologies or fast moving nuclei (g). The combined treatment with ML7 and Y27632 results in bipolar morphologies in a larger population of cells (h). Phase contrast images, scale bar: 100μm. See also movies 3-6.
494x700mm (72 x 72 DPI)

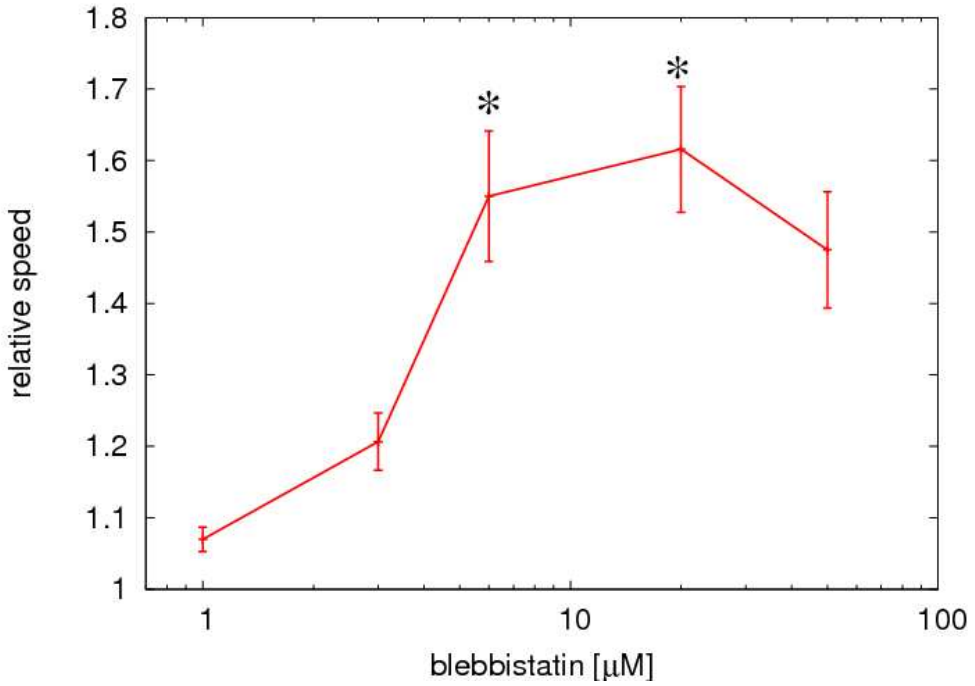

Normalized speed of nucleus movements in C6 cells as a function of blebbistatin concentration. Myosin II inhibition provokes increased nuclear motility even at relatively high concentration of blebbistatin. The population average speed of nuclei in blebbistatin treated cultures were normalized to similar averages obtained in parallel control cultures. The average nuclear speed in control cultures is 7 $\pm$ 0.6 μm/h (n=9 fields). Error bars represent SEM, calculated from independent microscopic fields (n=3 for 1 and 3 μM; n=4 for 6; n=9 for 20 μM; and n=2 for 50 μM. Significance values $p<0.05$ in two-sided t-tests were considered significant and marked by asterisks). Each analyzed field contained at least 100 tracked nuclei and more than 5000 nucleus positions.
254x177mm (72 x 72 DPI)

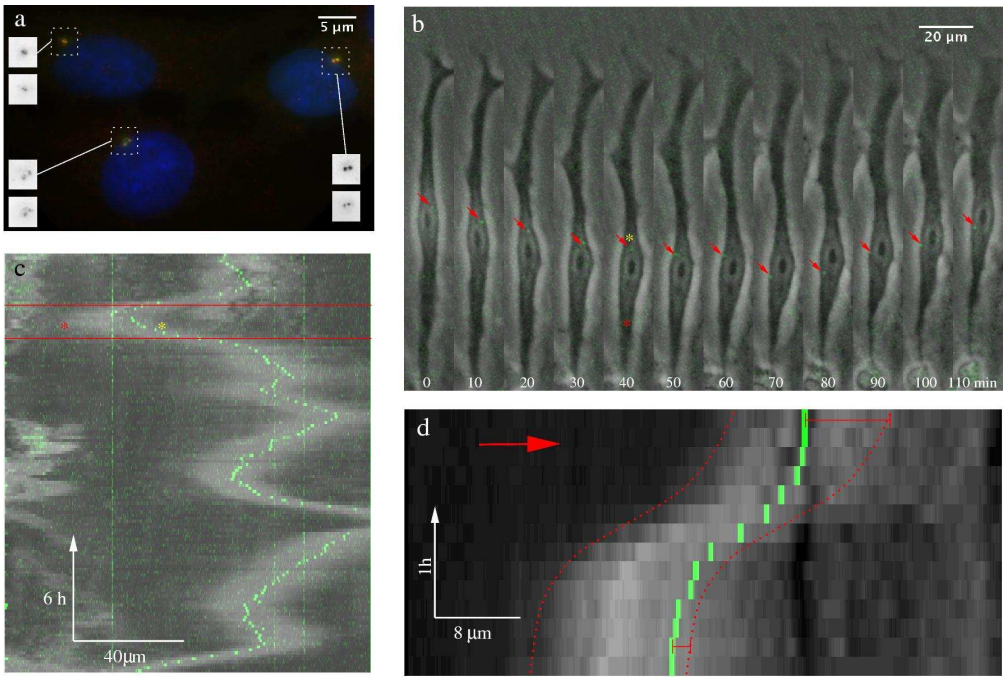

Centrosome position during nuclear movement in C6 cells. a: The centrosome is visualized by GFP-centrin epifluorescence (green) in a typical cluster of transfected C6 cells. Immunostaining with anti-centrin antibodies (red) gives exact co-localization (yellow) at the resolution of the 100X oil immersion objective. Nuclei are stained with a Hoechst reagent (blue). Insets show the red (top) and green (bottom) channels inverted for better contrast. b: A GFP-centrin transfected C6 cell, cultured on a 20 μm wide micropatterned fibronectin-coated stripe, is shown in consecutive time points. Grayscale phase contrast and green fluorescence time-lapse images were superimposed to show the centrosome position (see also movie 7). Red arrows point to the centrosome. Approximate edges of the bright halo (a phase contrast effect) surrounding the nucleus is marked by a red and a yellow asterisk. The image sequence depicts a reversal of nucleus direction. During this particular event, the centrosome moved suddenly relative to the nucleus (between frames taken at 60 and 70 minutes). c: Centrosome position during several nuclear oscillations. Intensity profiles were obtained by projecting the brightest pixels in the direction perpendicular to the long cell axis. Thus, a horizontal line of panel c corresponds to a single time-lapse frame, like those shown in panel b. Light gray areas reveal the position of the phase contrast halo surrounding the nucleus, green dots mark the centrosome. Frames shown in panel b correspond to the sequence between the red lines. Red and yellow asterisks label the same locations as in the frame at 40 min in panel b. Some, but not all nuclear turns contain a sudden relocation of the centrosome, similar to the event depicted in panel b. d: The nucleus tends to overtake the centrosome between the turns. Intensity profiles, similar to panel c, are depicting nuclear and centrosome movement between two nuclear direction reversals. The approximate leading and trailing nucleus boundaries are marked with red dotted lines. While the centrosome initially is at the front of the nucleus, it lags behind: the upper red bracket is longer than the lower one.
629x421mm (72 x 72 DPI)

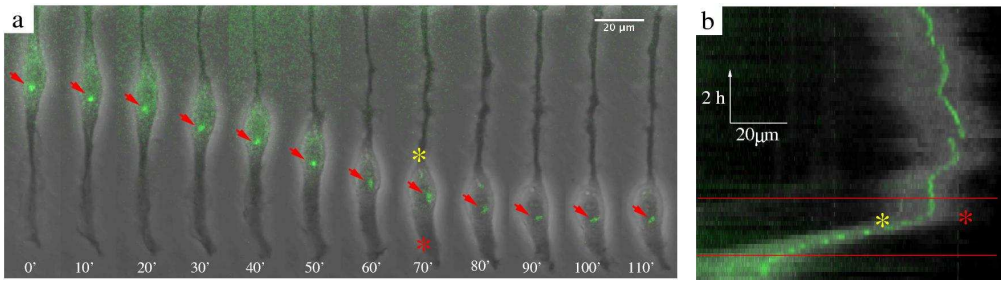

Centrosome position during blebbistatin-induced nuclear movement in C6 cells. a: The centrosome visualized by GFP-centrin epifluorescence in a typical transfected C6 cell treated with 20 μM blebbistatin. Grayscale phase contrast and green fluorescence time-lapse images were superimposed to show the centrosome position (See also movie 8). Red arrows point to the centrosome. Approximate edges of the bright halo (a phase contrast effect) surrounding the nucleus is marked by a red and yellow asterisk. b: Centrosome position during nuclear movement, plotted as in Fig 4c. Frames shown in panel a correspond to the area between the red lines. Red and yellow asterisks mark the same locations as in panel a. The centrosome tends to be in front of a moving nucleus. We did not observe rapid alterations in the direction of blebbistatin-induced nuclear motility.
617x170mm (72 x 72 DPI)

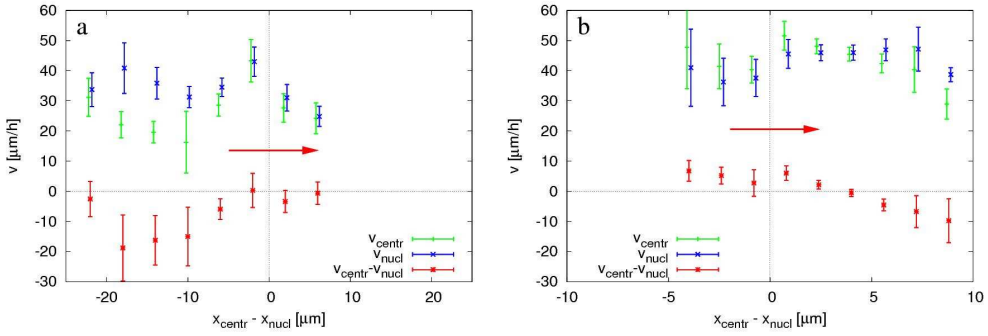

Average organelle speeds as a function of centrosome position, in untreated (a) and 20 μM blebbistatin-treated cultures (b). Speed of the nucleus (blue) and the centrosome (green) are plotted together with their relative speed (red). The presented data includes only cells in which the nucleus moved faster than 5 μm/h and where the centrosome was detectable. At least 160 data points were binned and averaged based on the relative position of the centrosome along the cell axis. Speed and position values were obtained by projecting the two dimensional vector quantities to the direction of nuclear movement. Speed values reflect instantaneous movements, calculated from displacements during 10 minutes. The more compact nucleus and cell body of blebbistatin-treated cells is reflected by the smaller scale of position differences in panel (b). The velocity of the two organelles are very similar, a consequence of the fact that in C6 cells the nucleus and the centrosome remain in close proximity. Error bars represent SEM. Direction of nuclear movement is indicated by horizontal red arrows.
633x221mm (72 x 72 DPI)

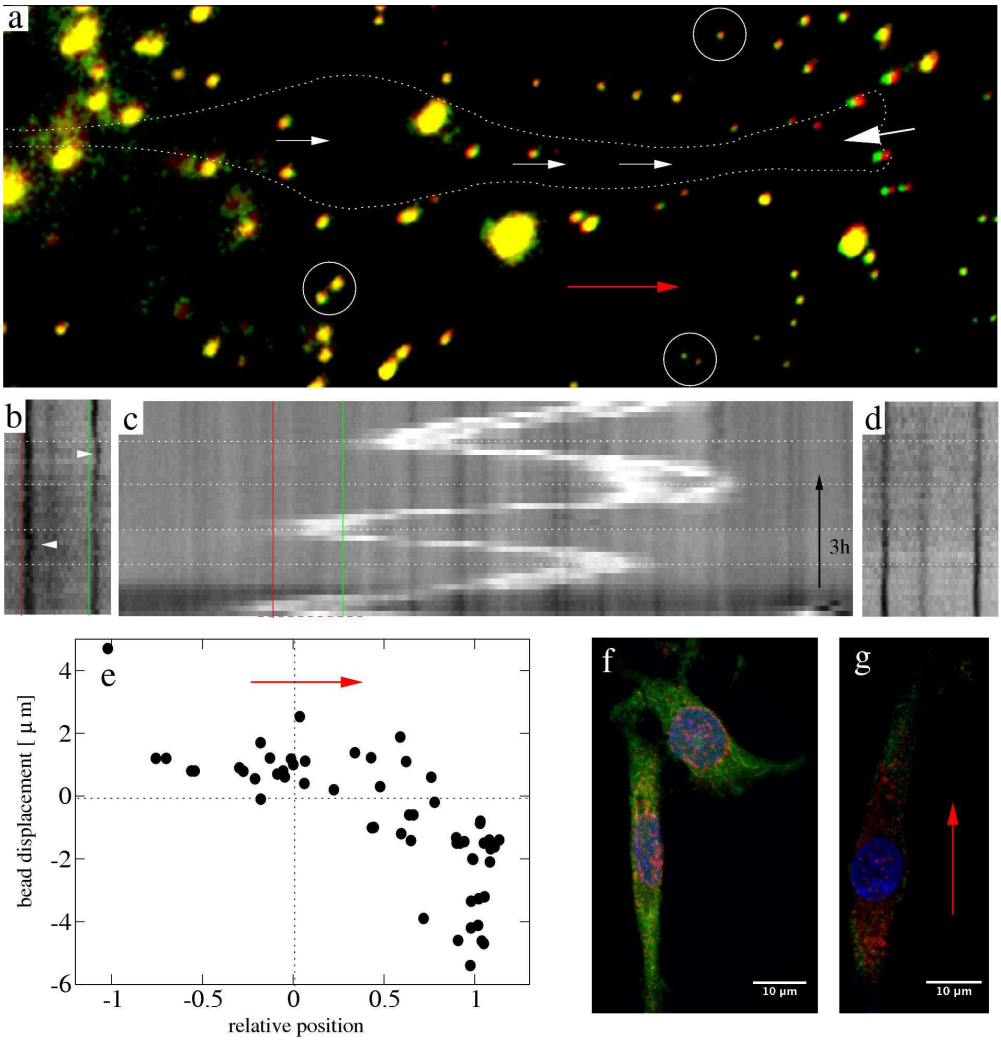

Substrate deformations indicate a contraction between the leading edge and the nucleus during nuclear movement in spontaneously elongated C6 cells. a: Bead positions (green) during nuclear movement of a cell outlined with dotted line, superimposed upon the stress-free configuration obtained by trypsin treatment (red). Substantial bead displacements, characterized by the lack of colocalization of green and red colors, are visible at the leading edge (large white arrow). Displacements of smaller magnitude characterize the area surrounding the nucleus (small white arrows). Beads far from the cell show no displacement (circles). The direction of nuclear movement is indicated by the red arrow. Bead aggregates yield larger fluorescent blobs. b-d: Intensity profiles, obtained as in Fig.~4c, of a typical oscillating cell show that bead displacements (b) change in synchrony with the direction of nuclear movements (c). The nucleus appears as a bright stripe and horizontal dotted lines are visual guides, denoting phases of oscillating nuclear movement. The vertical red and green lines, separated by 10 μm, mark the same location in both (b) and (c). Arrowheads point to bead displacements. Beads far from the cell show no displacements during the same time interval (d). e: Bead displacements, pooled from n=6 cells, are plotted against their relative position along the front/rear axis of the cell. The zero and unit abscissa values denote the nucleus and the leading edge, respectively. Positive displacements are parallel to the direction of cell movement, indicated by the red arrow. f: Immunocytochemical localization of pMLC (red) in C6 cells, superimposed upon images of phalloidin-labeled filamentous actin (green) and a Hoechst nuclear stain (blue). The distribution of pMLC labeled foci is quite symmetric in both well spread and

elongated cells. The vicinity of the nucleus is the source of the most intense pMLC immunofluorescence. g: Immunocytochemical localization of pMLC (red) superimposed upon images of vinculin immunofluorescence (green) and a Hoechst nuclear stain (blue). A C6 cell is shown in which the nucleus moved intensively in the direction marked by the red arrow. pMLC can be found both in the front and in the rear of the nucleus. The viculin immunostaining indicates the presence of scattered small adhesion sites instead of extended focal contacts characteristic of fully spread C6 cells in culture.
675x697mm (72 x 72 DPI)

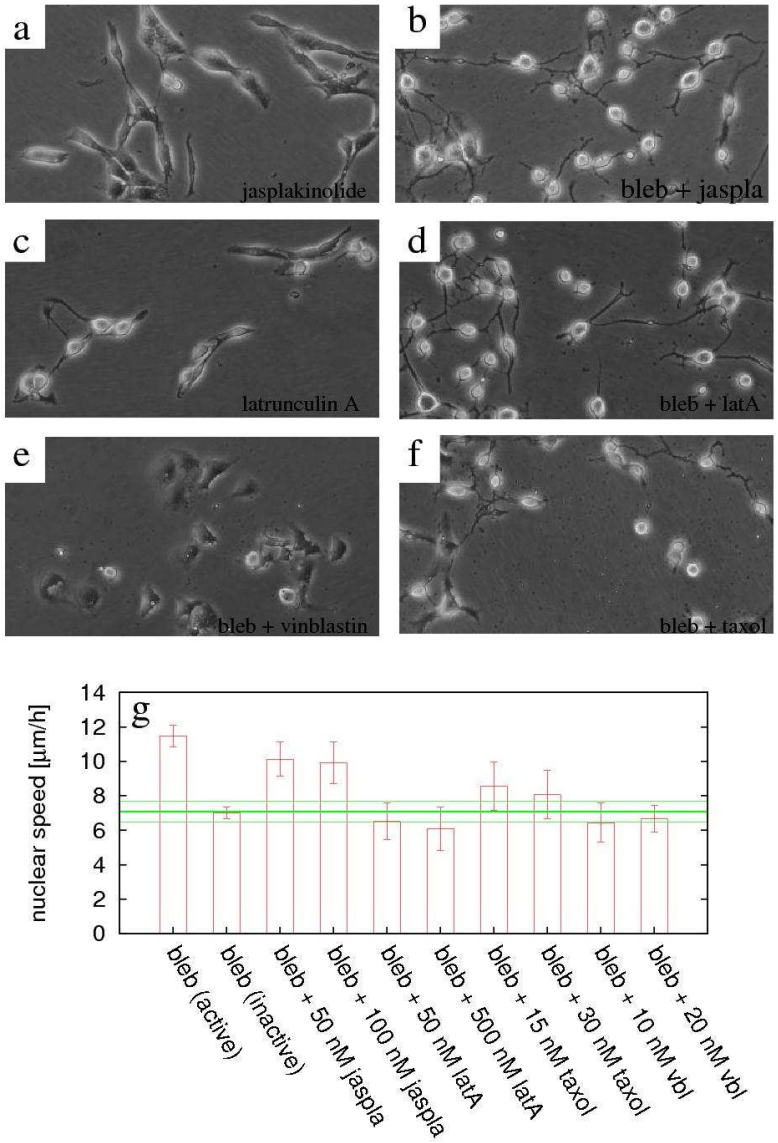

The role of normal cytoskeletal turnover in nuclear motility. C6 cells are exposed to microtubule and F-actin stabilizing and destabilizing agents: taxol, vinblastin, jasplakinolide and latrunculin A. Characteristic cell morphologies are shown for 100 nM jasplakinolide (a), together with 20 μM blebbistatin (b); 50 nM latrunculin A (c), together with 20 μM blebbistatin (d); and 20 nM vinblastine (e) and 30 nM taxol (f) together with 20 μM blebbistatin. g: Population and time-averaged nuclear speeds, obtained by automatic tracking, are compared to that of untreated cultures at 7 ± 0.6 μm/h (green lines). Blebbistatin concentration is 20 μM. The labels jaspla, latA and vbl indicate jasplakinolide, latrunculin A and vinblastine, respectively. Error bars represent standard error of the mean. See also movies 9 and 10.
329x507mm (72 x 72 DPI)

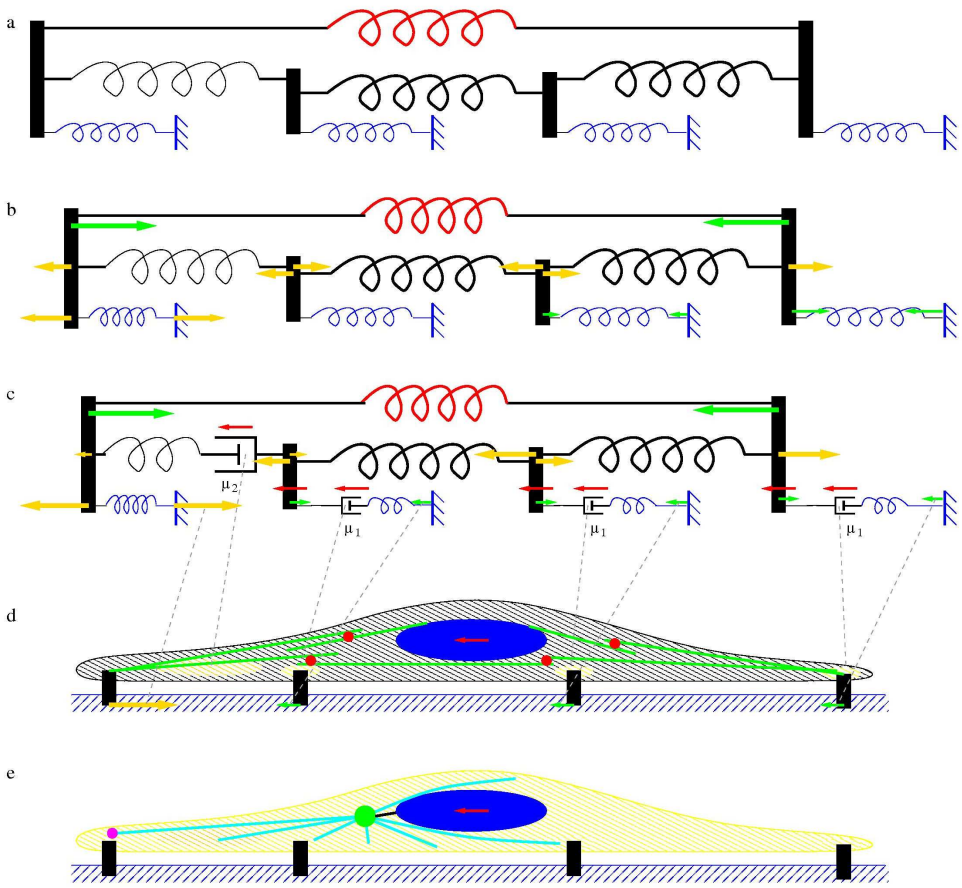

Schematic model of cytoskeletal dynamics during nuclear movements. We consider a system of an active contractile element (red spring) and a chain of passive elements (black springs) attached to an elastic environment (blue objects). a: If the active element is turned off, no forces are present in the system. b: When the active element contracts, this force is balanced by the compression of the passive elements and deformation of the environment. Forces exerted by the elements are represented by arrows. Compression and tension of the elements is indicated by yellow and green vectors, respectively. We assume that the passive element in the front (the spring drawn with a thinner line) is more compliant, which creates an uneven compression pattern and a matching asymmetry in forces within the environment (forces exerted by the blue springs). c: To accommodate a sustained movement of a large part of the structure (red arrows) we introduce elements, represented by dashpots, which can dissipate mechanical stress. The spring and dashpot in a serial arrangement models the cytoskeleton as a viscoelastic Maxwell fluid. The dissipative elements couple the speed of movement and the force exerted upon the element, the conversion factors are marked as μ_1 and μ_2. Forces can be established by requiring mechanical equilibrium and the co-movement of the elements marked by red arrows. d: The elements shown in panel c are represented within a cartoon of a contractile cell. Traction forces exerted by the cell are marked as vectors and matched with the corresponding forces by dashed gray lines. The passive cytoskeleton is represented as a hatch pattern. Areas where we assume intensive dissipation of mechanical tension (remodeling) are marked yellow and matched by the corresponding dashpots with gray dashed lines. The active contractile elements are shown as green lines (actin filaments) and red disks (myosin II motors). e: In the absence of myosin II activity, the cytoskeleton is more compliant, and we envision a microtubule-based mechanism to move the nucleus: Cortical motors (magenta) pull the astral microtubules (cyan) and the centrosome (green disk), which in turn, is

linked (thick black line) to the nucleus. This mechanism may operate in parallel with the myosin II dependent contractility shown in panel d.
810x755mm (72 x 72 DPI)